# Annealing Induced Structural Evolution in Feldspar Dental Glass-Ceramics Investigated by Solid-State NMR Spectroscopy

Amit Bhattacharya [a], Yu Qiu [a], Guy M. Bernard [a], Sheila Butler [b], Arthur Mar [a], and Vladimir K. Michaelis [a,*]

[a] *Department of Chemistry, University of Alberta, Edmonton, Alberta, Canada T6G 2G2*

[b] *Schulich School of Medicine and Dentistry, Western University, London, Ontario, Canada N6A 5C1*

[*]Corresponding author: vladimir.michaelis@ualberta.ca

*Keywords*: Glass-ceramic; Feldspar; Dental Material; Solid-state NMR

**Abstract**

Glass-ceramics are an attractive oxide-based material routinely used for biomineral repair such as porcelain veneers in dental crown applications. The short- and long-range structure of a commercial glass-ceramic feldspar material, VITA VM9, has been investigated as a function of annealing temperature. The relative amounts of amorphous and crystalline components were monitored using a combination of powder X-ray diffraction and solid-state $^{23}$Na, $^{27}$Al, and $^{29}$Si nuclear magnetic resonance spectroscopy. The insight gained from this study was then applied to analyze a series of synthetic lab-grade ceramics $Na_{0.5}K_{0.5}Al_{1-x}M_xSi_3O_8$ ($x$ = 0.1; $M$ = B, Al, Ga), whose onset of crystallization was found to resemble that of the commercial ceramic material.

## Introduction

Feldspars are naturally occurring framework aluminosilicate minerals having compositions that are generally based on solutions of the end-members $NaAlSi_3O_8$ (albite), $KAlSi_3O_8$ (orthoclase), and $CaAl_2Si_2O_8$ (anorthite). Synthetic feldspars have many industrial applications. In particular, they are widely used as glass-ceramic dental materials (crowns, implants, and veneers) because they retain the esthetically pleasing appearance of natural teeth while showing good performance characteristics. The attractive optical properties are conferred by an amorphous glassy component, and the robust mechanical and corrosion-resistant properties are conferred by a crystalline ceramic component [1–4]. The properties of these synthetic materials depend on the degree of solid solution and the relative amounts of amorphous vs crystalline components [5,6]. Unfortunately, commercial veneers made of feldspars are prone to fracture along the ceramic-core interface, and 15% of them suffer from chipping within two years. These failures are attributed to microcracking, mismatches in the thermal expansion coefficients and elastic modulus between the porcelain and zirconia core [7–9], a weak bond at the zirconia-porcelain interface, poor porcelain veneer strength, restoration design, and annealing procedure [1,10–12]. To improve the properties of these materials, a deeper understanding of the structural details at varying annealing temperatures is essential.

The structures of glass-ceramic materials are challenging to analyze precisely because they contain both amorphous and crystalline components. Short- and long-range order are important to determine, but no one technique can accomplish this alone. However, the structure of a glass-ceramic material can be elucidated through the complementary techniques of powder X-ray diffraction (XRD), which probes the long-range order present in the crystalline portion, and solid-state nuclear magnetic resonance (NMR) spectroscopy, which probes the local environments

around individual atomic sites [13,14]. Previous studies of aluminosilicates, including feldspars, by solid-state NMR spectroscopy, have illustrated its utility in providing characteristic signatures that are related to the degree of Al/Si disorder, in distinguishing between crystalline vs amorphous components, and in revealing other details of bonding [15–21].

Magnetic shielding and quadrupolar coupling are two prominent NMR interactions that offer sensitive markers to qualitatively and quantitatively assess natural and synthetic minerals. The most important interaction is the chemical shift, because it is extremely sensitive to the coordination environment and neighbouring species within various crystalline and amorphous oxides [22–26]. NMR-active nuclei having a nuclear spin of $I > ½$ can further assist in assessing local and medium-range structure when they exhibit a non-zero electric field gradient (EFG), which couples to the intrinsic quadrupole moment of the NMR-active nucleus. The resulting nuclear quadrupole interaction provides further information through characteristic lineshapes and breadths [27,28].

Herein, we examine the effect of annealing temperature on the structural evolution and the relative degrees of crystalline and amorphous components in a commercial dental material (VITA VM9) and in several synthetic feldspar materials using powder XRD and solid-state NMR spectroscopy. To assess how the network-forming and network-modifying cations affect the structural features, 1D and 2D NMR experiments were conducted at high (14.1 T) and ultrahigh (21.1 T) fields. The ultrahigh-field experiments led to improved resolution, enabling the relative amounts of crystalline and amorphous components to be quantified. This study demonstrates that a multinuclear, ultrahigh-field magnetic resonance approach can offer additional insights into the structures of glass-ceramic materials and may help unravel complex structure-property relationships.

## Experimental

*Commercial materials.* Commercial dental ceramic VITA VM9 was obtained from Vita Zahnfabrik, Germany. The bulk powder was cold-pressed into several pellets, each of which was placed in a Pt–Au (95%/5%) crucible and heated to various set temperatures (ranging from 600 to 1100 °C) for 18 h in a box furnace, followed by cooling to room temperature.

*Synthetic materials.* A synthetic sample of $Na_{0.5}K_{0.5}AlSi_3O_8$ feldspar was prepared from a stoichiometric mixture of $Na_2CO_3$ (99.5%, Alfa-Aesar), $K_2CO_3$ (99.9%, Sigma-Aldrich), $Al_2O_3$ (99.5%, Sigma-Aldrich), and $SiO_2$ (>99%, Sigma-Aldrich), which were ground finely for 30 min in an agate mortar. The mixture was cold-pressed into a pellet and heated from 700 to 1100 °C stepwise in 100 °C increments over five days. The product was subsequently reground, pressed into a pellet, and annealed at 900 °C overnight. B- and Ga-substituted samples were prepared in an identical manner, except that 10% of $Al_2O_3$ was replaced by either $B_2O_3$ (99.9%, Sigma-Aldrich) or $Ga_2O_3$ (99.9%, Sigma-Aldrich).

*X-ray diffraction.* Powder XRD patterns were collected on an Inel powder diffractometer equipped with a curved position-sensitive detector (CPS 120) and a Cu $K\alpha_1$ radiation source operated at 40 kV and 20 mA. Le Bail profile fitting was carried out as implemented in the FullProf software suite [29]. Diffraction peaks located at $2\theta = 37°$ and 43° are a background artefact from the sample holder and not from the dental glass-ceramics.

*SEM and EDX analysis.* Scanning electron microscopy imaging and energy-dispersive X-ray (EDX) analyses were performed on a JEOL JSM 6010LA InTouchScope scanning electron microscope, operated with an accelerating voltage of 10 kV.

*Solid-state NMR spectroscopy.* Silicon-29 magic angle spinning (MAS) NMR spectra were collected on a Bruker Avance 300 MHz NMR spectrometer equipped with a double resonance 4-

mm MAS probe, using a short tip angled (~10°) Bloch pulse ($\gamma B_1/2\pi$ = 62.5 kHz), recycle delay of 40 s, and 3000–6000 co-added transients. To ensure that spin-lattice relaxation did not impact the results described, a series of experiments was performed in which the recycle delay was varied from 30 to 1200 s. As shown (Figure S1), few changes were observed in the overall intensities. The presence of small paramagnetic impurities within these oxides assists nuclear relaxation through paramagnetic relaxation, enabling quick recycle delays when combined with short pulse widths. Nevertheless, we refrain from peak-fitting the $^{29}$Si NMR results. All compounds were ground using an agate mortar and pestle, packed in $ZrO_2$ rotors (4 mm o.d.), and spun at a frequency of 5 kHz. The spectra were referenced to TMS ($\delta$ = 0) by setting the high-frequency peak of tetrakis(trimethylsilyl)silane to –9.8 ppm. The $^{11}$B, $^{23}$Na, $^{27}$Al, and $^{71}$Ga MAS NMR spectra were collected on an Agilent VNMRS 600 MHz NMR spectrometer equipped with a triple resonance (HXY) Varian MAS probe, using a Bloch pulse of 0.2 to 1.0 μs (tip angles of 7° for $^{23}$Na, 11° for $^{27}$Al, 33° for $^{71}$Ga, and 12° for $^{11}$B), a recycle delay between 1 and 3 s, 2000–5000 co-added transients, and a spinning frequency of 16 kHz. Spectra were referenced to 0.1 M NaCl (0 ppm, $^{23}$Na), 1.1 M $AlCl_3$ (0 ppm, $^{27}$Al), 0.1 M $H_3BO_3$ (+19.6 ppm, $^{11}$B), or 1.1 M $Ga(NO_3)_3$ (0 ppm, $^{71}$Ga). All NMR experiments were performed under ambient conditions [19].

Ultrahigh-field $^{23}$Na and $^{27}$Al MAS NMR spectra were collected on a Bruker Avance II 900 MHz NMR spectrometer equipped with a double resonance Bruker probe. Samples were packed into 2.5 mm $ZrO_2$ rotors and spun at a frequency of 31.25 kHz. Sodium-23 NMR spectra were acquired using a Bloch pulse of 0.5 μs (tip angle of 30°), 512 co-added transients, and a recycle delay of 1 s. Aluminum-27 NMR spectra were acquired using a Bloch pulse of 0.3 μs (tip angle of 30°), 256 co-added transients and a recycle delay of 1 s. Multiple quantum (3Q) MAS NMR spectra were acquired using a three-pulse z-filtered sequence. Each pulse was optimized for

maximum transfer efficiency ($^{23}$Na: P1 = 4 μs, P2 = 1.5 μs, P3 = 10 μs and $^{27}$Al: P1 = 2.6 μs, P2 = 0.9 μs, P3 = 10 μs). The $^{23}$Na 3QMAS data were acquired using a 0.4 s recycle delay, 2048 scans, and 96 $t_2$ increments set to four times the rotor period. The $^{27}$Al 3QMAS data were acquired using a 2 s recycle delay, 96 scans, and 128 $t_2$ increments set to two times the rotor periods. Spectra were processed using TOPSPIN software (Bruker) and between 50 and 300 Hz exponential apodization.

**Results and Discussion**

Among many factors that influence the structure and properties of synthetic feldspars, the heat treatment applied during synthesis is poorly understood and forms the focus of the present study. How the heat treatment affects the evolution from disordered (amorphous) to semi-ordered structures (glass-ceramic) in a commercial dental ceramic and related synthetic materials can be tracked by diffraction and spectroscopic methods.

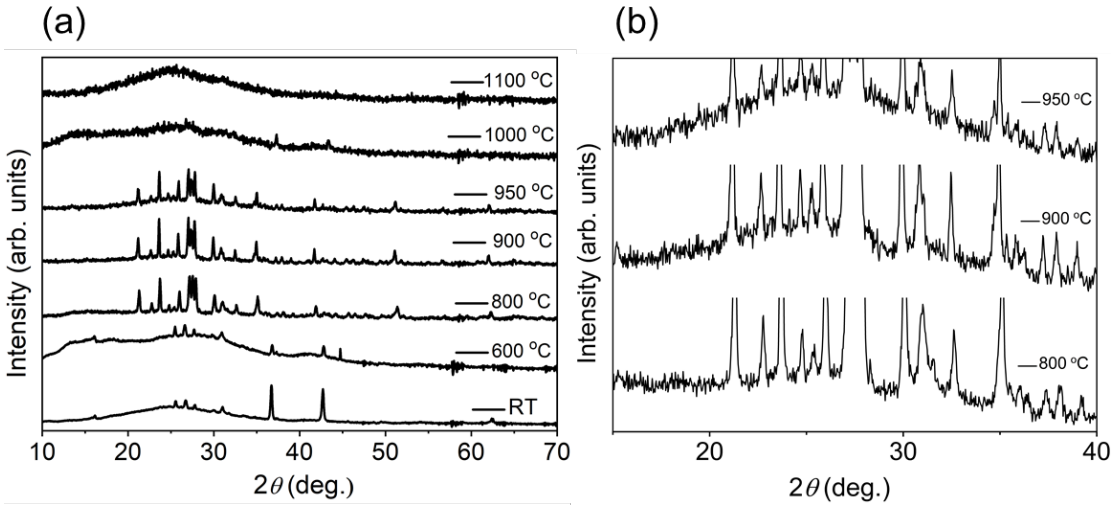


**Figure 1.** (a) Powder XRD patterns of dental ceramic VITA VM9 treated at different temperatures. (b) Expanded view for patterns at 800, 850 and 900 °C revealing an underlying broad component. (Diffraction peaks located at 37° and 43° in 2$\theta$ are an artefact from the sample holder.)

*Evolution of crystalline component.* Separate samples of the commercial dental material VITA VM9 were treated at various temperatures between 600 and 1100 °C and examined by powder XRD (Figure 1a). In general, the broad humps in these patterns are attributed to an amorphous component and the sharp peaks to a crystalline component. At room temperature, the untreated starting material is largely amorphous. No drastic changes are observed between room temperature and 600 °C. Above 600 °C, the broad hump begins to be suppressed by the sharp peaks, indicating that a gradual rearrangement of atoms is taking place, inducing ordering and indicating the onset of crystallization. The sharp peaks begin to dominate between 800 and 950 °C, indicating increased ordering. Close examination of the XRD patterns reveals that a broad background remains at these temperatures (Figure 1b), indicating that some amorphous component is always present as part of the dental material. Above 1000 °C, all crystallinity is lost and a liquid melt forms, as confirmed by visual inspection of the sample when it was removed from the furnace. Upon melting, the sample transforms into a glass, which lacks long-range periodic order and is manifested as a broad hump in the XRD pattern at 1100 °C.

Lattice parameters of the crystalline component were obtained from the profile fitting of the XRD patterns between 800 and 950 °C (Table S1). Na-rich feldspar, $NaAlSi_3O_8$, crystallizes in a triclinic (nearly monoclinic) form, whereas K-rich feldspar, $KAlSi_3O_3$, exists in both triclinic and monoclinic forms. The commercial dental material is found to adopt the triclinic form as shown in Figure 2, consistent with the composition $Na_{0.5}K_{0.5}AlSi_3O_8$ as revealed by EDX analysis (Table 1).

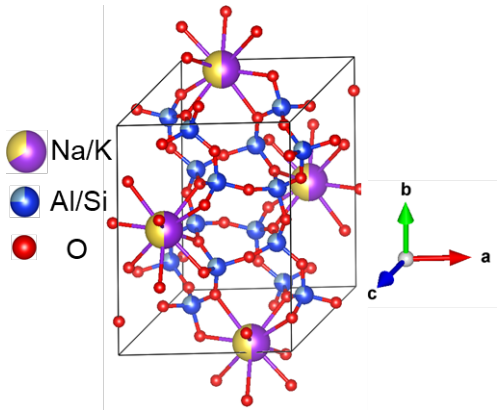


**Figure 2.** Crystal structure of $Na_{0.5}K_{0.5}AlSi_3O_8$ (triclinic).

**Table 1.** EDX analyses (mol%) of commercial and lab-grade dental ceramics.

| | VITA VM9 | $Na_{0.5}K_{0.5}AlSi_3O_8$ | $Na_{0.5}K_{0.5}Al_{0.9}Ga_{0.1}Si_3O_8$ |
|---|---|---|---|
| Na | 9(1) | 9(1) | 10(1) |
| K | 13(5) | 10(4) | 10(5) |
| Al | 16(1) | 19(1) | 15(2) |
| Ga | | | 3(1) |
| Si | 62(2) | 62(2) | 62(2) |

The effect of annealing on the morphology of the samples was examined by SEM (Figure S2). As the temperature increases, the particles increase in size and become more uniform in shape. At 1100 °C, the surfaces are smooth, which indicates that melting has occurred, as corroborated by the XRD patterns and NMR spectra.

*Network-forming oxides.* In glass science, oxide components are often classified into network-forming species (e.g., $SiO_2$, $B_2O_3$, $Al_2O_3$), which build up the structure, and network-modifying species (e.g., alkali and alkaline-earth cations), which disrupt the polymerized network to form non-bridging oxygen atoms and which compensate for the charge of the anionic network to maintain overall charge neutrality. NMR spectroscopy is a robust method to probe the local structure of glasses by detecting changes in coordination environments and neighbouring cations

which would otherwise be invisible using other tools. The presence of a broad amorphous feature in the powder XRD patterns of the dental ceramic warrants further investigation by $^{29}$Si and $^{27}$Al MAS NMR spectroscopy.

$^{29}$Si NMR spectroscopy ($I$ = ½; 4.7 % natural abundance) is well suited to characterize aluminosilicates [14,30], with the ability to reveal second-coordination environments based on the Al substitution pattern around four-coordinate Si with all bridging oxygens, denoted as $Q^4$. There are five types of possible environments around the Si atoms, ranging from zero ($Q^4$(0Al)) to four Al neighbours ($Q^4$(4Al)) within the second coordination sphere. The ranges of chemical shifts for these Si environments are approximately −102 to −116 ppm for $Q^4$(0Al), −97 to −107 ppm for $Q^4$(1Al), −92 to −100 ppm for $Q^4$(2Al), −85 to −94 ppm for $Q^4$(3Al), and −82 to −92 ppm for $Q^4$(4Al) [14]. The gradual trend in the chemical shift to a higher frequency with the greater number of Al atoms serves to identify the type of silicate species present in the feldspar. Some overlap occurs in these chemical shift ranges and is exacerbated by the broader resonances often associated with the disordered structures of feldspars. The diminished resolution results from the distribution of chemical shifts arising from the varying T-site bond lengths and angles caused by Si/Al and Na/K disorder.

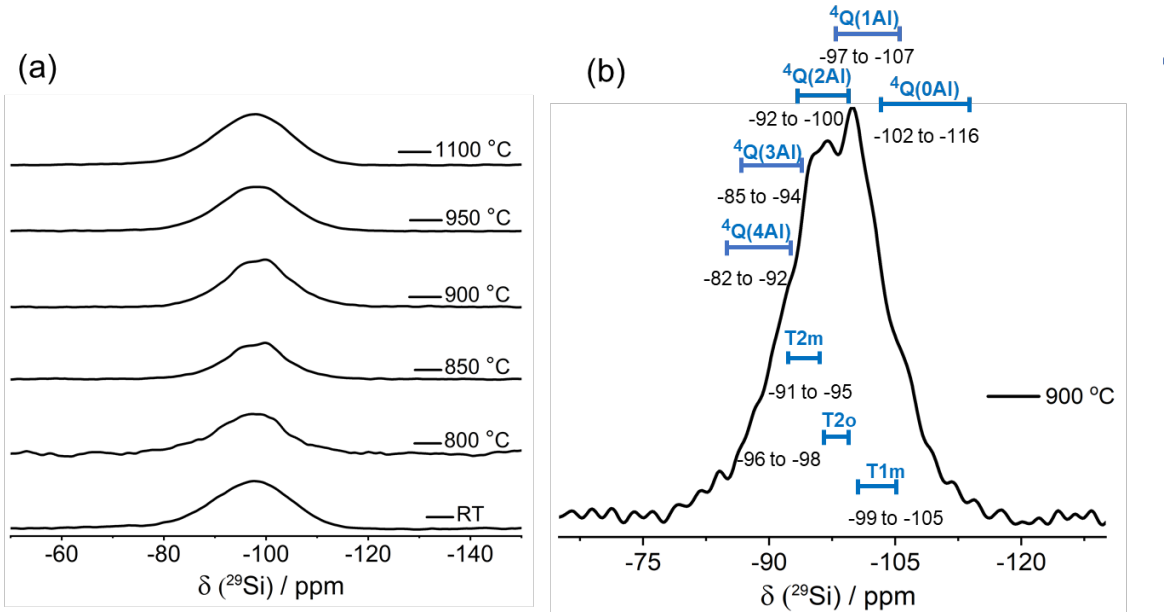


**Figure 3.** (a) $^{29}$Si MAS NMR spectra ($B_0$ = 7.05 T) for dental ceramic VITA VM9. (b) Expanded view of the spectrum for the sample treated at 900 °C, with assignments based on ref. 15.

$^{29}$Si MAS NMR spectra ($B_0$ = 7.05 T) were collected for the same series examined earlier by powder XRD (Figure 3). They show a broad Gaussian-like resonance spanning from −85 to −110 ppm, consistent with an overall amorphous structure. These results are consistent with previous NMR studies of natural feldspar minerals, which can range from well-resolved data, with three distinct Si resonances appearing at −102 ± 2 ppm (T1m), −97 ± 2 ppm (T2o), and −91 ± 2 ppm (T2m) in highly ordered structures, to the collapse of these signals into a single, broad Gaussian-like resonance [15,16,31,32]. For the dental ceramic studied here, there are four crystallographically inequivalent T-sites, each of which could experience second coordination environments varying between zero to four Al neighbours. Thus, there are a total of 20 possible Si chemical environments. The large variation in Si environments in a glass or glass-ceramic would lead to a broad $^{29}$Si signal spanning a wide range of chemical shifts. If Lowenstein's rule is obeyed (i.e., no $^{[4]}$Al-O-$^{[4]}$Al linkages are permitted) and the stoichiometric ratio of network-forming

cations (1 Al : 3 Si) is considered, then the most probable medium-range Si chemical environments have one to two Al neighbours [33].

At room temperature and above 1000 °C, the spectra are dominated by the broadest Gaussian-like lineshapes of the amorphous component. The broad resonance encompasses the range of expected chemical shifts for $Q^4$(2Al), and $Q^4$(1Al) sites (and possibly others), and are consistent with the Na/K-feldspar structures [16,30,34]. Between 800 and 950 °C, there is a perceptible narrowing of the lineshapes and a slight shift in peak positions, suggesting that ordering is being induced. At 850 and 900 °C, multiple resonances begin to emerge from the broad resonance and are tentatively assigned to T1m, T2o, and T2m regions (Figure 3b). Altogether, these spectra provide evidence for the occurrence of intermediate Al–O–Si ordering and for the presence of Si in both amorphous and crystalline components of the glass-ceramic material. The underlying broad resonance and insufficient resolution inhibit a quantitative analysis of the amorphous and crystalline components, but they are consistent with the presence of significant amounts of the amorphous component, as indicated by the powder XRD results discussed earlier. The slight narrowing and emergence of three Si environments is also consistent with the XRD data, where the onset of crystallization was observed to occur between 800 and 950 °C.

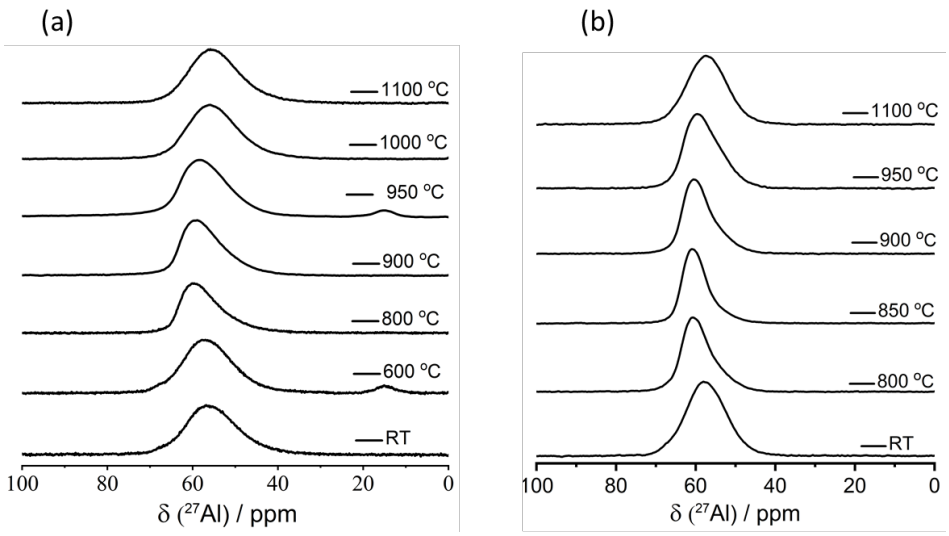


**Figure 4.** Aluminum-27 MAS NMR spectra for dental ceramic VITA VM9 subjected to various heat treatments, collected at (a) $B_0$ = 14.1 T and (b) $B_0$ = 21.1 T.

To examine the network further, $^{27}$Al NMR spectroscopy ($I$ = 5/2; 100 % natural abundance) was used to monitor changes in chemical shift and quadrupolar interaction, as aluminium can reside in any of the T-sites in crystalline feldspars. The $^{27}$Al MAS NMR spectra ($B_0$ = 14.1 and 21.1 T) are shown in Figure 4. At either extreme of the temperature range, the spectra show a broad Gaussian-like resonance with a distribution in chemical shifts caused by the amorphous nature of these materials. The overall resonance spans 30 ppm across a range from 40 to 70 ppm, consistent with a four-coordinate Al chemical environment ($^{[4]}$Al) [11,17,18]. Examination of the ultrahigh-field $^{27}$Al NMR spectra between −10 and 40 ppm reveals no evidence of higher coordinated aluminum chemical species ($^{[5]}$Al & $^{[6]}$Al), with the exception of the annealed samples at 600 and 950 °C, where a low intensity peak assigned to $^{[6]}$Al is attributed to a minor amount of $Al_2O_3$. This implies that nearly all the $^{[4]}$Al sites within the network are formed by $^{[4]}$Al–O–$^{[4]}$Si linkages (considering Lowenstein's Al avoidance rule) [33].

When the data at 14.1 and 21.1 T are combined, the extraction of random slices from the $^{27}$Al MQMAS spectra (*vide infra*) reveals a gradual reduction of the quadrupole coupling constant from $C_Q$ = 3.8 ± 0.4 (RT/melt) to 3.1 ± 0.2 MHz (900 °C), associated with a reduction in the distribution of quadrupolar parameters, consistent with the onset of crystallization. Past studies have reported $C_Q$ values between 3.1 and 3.3 MHz for Na/K feldspars minerals [16]. Between the critical annealing temperatures of 800 and 950 °C, the $^{27}$Al central transition narrows, with evidence of an asymmetric tail extending toward lower frequency, which is caused by a quadrupolar interaction whereby a distribution of EFGs becomes apparent as crystallization is induced. This is further supported by the 2D $^{27}$Al MQMAS, below, where the dominant distribution in chemical shifts is reduced in this range [35,36]. Although averages of quadrupole coupling constants are reported here, we note that there is a significant distribution in the $C_Q$ values that have been reported for a series of solid solutions (Na/K feldspars); as such, a distribution of both smaller and larger $C_Q$ values (upwards to 5.5 MHz) are required to effectively simulate these lineshapes. This result is consistent with a substantial variation in the Al T-site (T1o), and consequently, supports the broad $^{29}$Si resonances observed where Si variations also cause the wide distribution in chemical shift noted above [15].

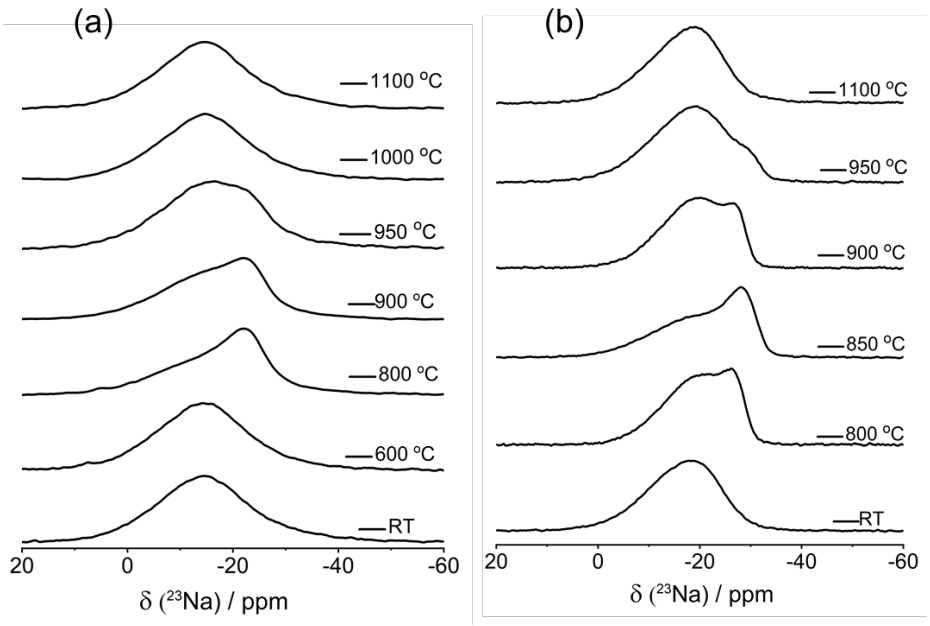


**Figure 5.** $^{23}$Na MAS NMR spectra for dental ceramic VITA VM9 subjected to various heat treatments, collected at (a) $B_0$ = 14.1 T and (b) $B_0$ = 21.1 T.

*Network-modifying oxides.* The dental ceramic material contains two network-modifying cations, $Na^+$ and $K^+$, which can serve as analytical markers to assess the relative degrees of amorphous vs crystalline character. In principle, both of these cations can be probed, but $^{23}$Na is much more favourable ($I$ = 3/2; 100 % natural abundance and $\Xi$ = 26.45 %) than $^{39}$K ($I$ = 3/2; 93 % natural abundance and $\Xi$ = 4.67 %) for 1D NMR studies and provides an accessible avenue for 2D studies [19,37].

The $^{23}$Na MAS NMR spectra collected at 14.1 T indicate the presence of at least two unique Na chemical environments (Figure 5a). To improve spectral resolution by reducing the second-order quadrupole broadening and to boost sensitivity, NMR spectra were also collected at 21.1 T (Figure 5b). The RT and 1100 °C samples give nearly identical spectra with a broad $^{23}$Na resonance spanning nearly 30 ppm (between 0 and – 30 ppm), which is consistent with an average coordination sphere of eight to ten oxygen atoms. The lack of a defined second-order quadrupolar

lineshape implies that the breadth is dominated by a distribution of chemical shifts due to the amorphous component. When the sample is annealed between 800 and 950 °C, the spectra are highly asymmetric, with the formation of two distinct resonances having centre-of-gravity shifts ($\delta_{cgs}$) at –28 and –19 ppm. These can be assigned to the crystalline and amorphous components, respectively [15]. As the heat treatment temperature increases, the intensity increases for the peak at $\delta_{cgs}$ = –28 ± 1 ppm ($C_Q$ = 1.3 ± 0.1) attributed to the ordered (crystalline) component, but decreases for the peak at $\delta_{cgs}$ = –19±3 ppm ($C_Q$ = 2.3±0.3) attributed to the disordered (amorphous) component. This result provides a direct atomic-level method to quantify the relative amounts of crystalline and amorphous components present in the sample under different annealing conditions. The reduction in $C_Q$ and the change in chemical shift are consistent with $Na^+$ cations entering a more symmetric environment made possible by the presence of $K^+$ cations. As has been previously reported, as the alkali-metal site expands, due to the introduction of larger $K^+$ cations, the overall Na–O distances increase, causing the bonding arrangement to become increasingly ionic and leading to a smaller electric field gradient, reducing $C_Q$ [15]. The fitted data used to quantify the crystalline and amorphous components are shown in Figure S3 and summarized in Table S2. Based on this quantitative analysis, an annealing temperature of 850 °C maximizes the degree of crystallinity, with ~29% of the glass-ceramic material exhibiting a crystalline component. At higher annealing temperatures, the crystalline component diminishes and gives way to greater amounts of the amorphous component.

Although the bulk glass-ceramic sample has an overall composition of $Na_{0.5}K_{0.5}AlSi_3O_8$, consisting of equal parts of Na and K, the characteristic shifts and quadrupolar coupling constants for the crystalline and amorphous features suggest that the crystalline portion is K-rich whereas the amorphous portion is Na-rich. This implies that the onset of crystallization is impacted not

only by temperature, but also by the partitioning of the network-modifying cations. Based on previous reports of Na/K feldspar solid solutions, we estimate that the crystalline component of the commercial dental material has a composition between $Na_{0.2}K_{0.8}AlSi_3O_8$ and $Na_{0.4}K_{0.6}AlSi_3O_8$, while the amorphous component accepts the excess Na [15].

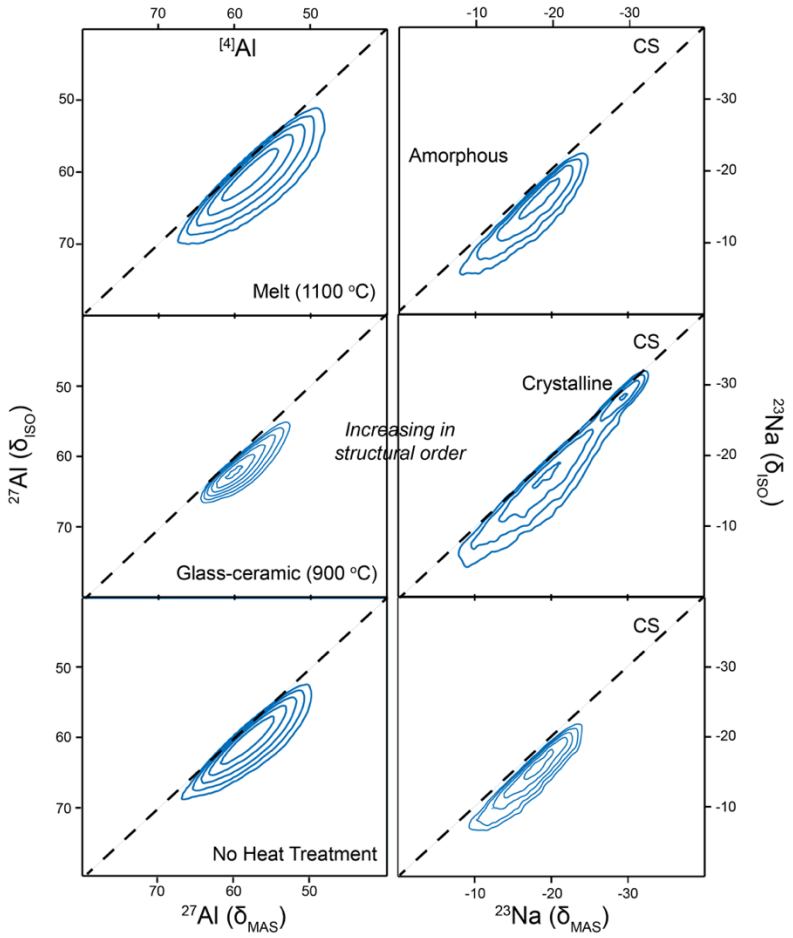


**Figure 6.** Triple quantum (3Q) $^{27}Al$ (left) and $^{23}Na$ (right) MAS NMR spectra ($B_0$ = 21.1 T; $\omega_r/2\pi$ = 31.25 kHz) of dental ceramic VITA VM9 at 25 °C (bulk powder, no heat treatment), heat-treated at 900 °C, and quenched melt at 1100 °C. The chemical shift (CS) axis is marked by the dashed lines, and four-coordinate aluminum environment is abbreviated as $^{[4]}Al$.

The $^{27}Al$ and $^{23}Na$ NMR spectra of the commercial dental material are compared with spectra at 21.1 T simulated based on past results for crystalline $NaAlSi_3O_8$, $KAlSi_3O_8$, and $Na_{0.5}K_{0.5}AlSi_3O_8$ (Figures S4 and S5) [15]. As expected, the parameters for the dental material are

intermediate between those for $NaAlSi_3O_8$ and $KAlSi_3O_8$. However, the dental material shows much broader spectra than the end-members, confirming a high degree of structural disorder arising from the Na/K mixing and the distribution of sites within the amorphous component. To verify that no further sites are hidden underneath the spectra, additional MQMAS experiments were performed (Figure 6). In general, the MQMAS spectra are consistent with the corresponding 1D ultrahigh-field NMR spectra discussed above, with a single Al site and two distinct Na sites. The onset of crystallization is accompanied by a reduction in the CS distribution in the $^{27}Al$ MQMAS spectra, while crystalline and amorphous components are resolved in the $^{23}Na$ MQMAS spectra. The amorphous nature of the RT and 1100 °C samples is manifested by a single resonance with a sizable distribution in chemical shifts, complementing the 1D NMR results. As indicated above, $^{23}Na$ NMR spectra are highly valuable for interrogating the degree of disorder induced by different heat treatments. Although the 1D NMR data at 21.1 T were sufficient to reveal these structural details, $^{23}Na$ MQMAS experiments are an attractive approach if access to higher field instrumentation is unavailable. The projected isotropic spectra are provided in Figure S6.

*Manipulation of glass-ceramic balance.* To determine if the proportions of amorphous and crystalline components in dental ceramics can be adjusted through synthetic modifications, we prepared a lab-grade ceramic with the same composition as the commercial material, $Na_{0.5}K_{0.5}AlSi_3O_8$, as well as the derivatives $Na_{0.5}K_{0.5}Al_{0.9}B_{0.1}Si_3O_8$ and $Na_{0.5}K_{0.5}Al_{0.9}Ga_{0.1}Si_3O_8$ in which 10% of the network-forming Al atoms was substituted by smaller B or larger Ga atoms. Except for the sample containing B (which cannot be detected by EDX analysis), these compositions were confirmed (Table 1). These samples were then subjected to a similar analysis as performed on the commercial material.

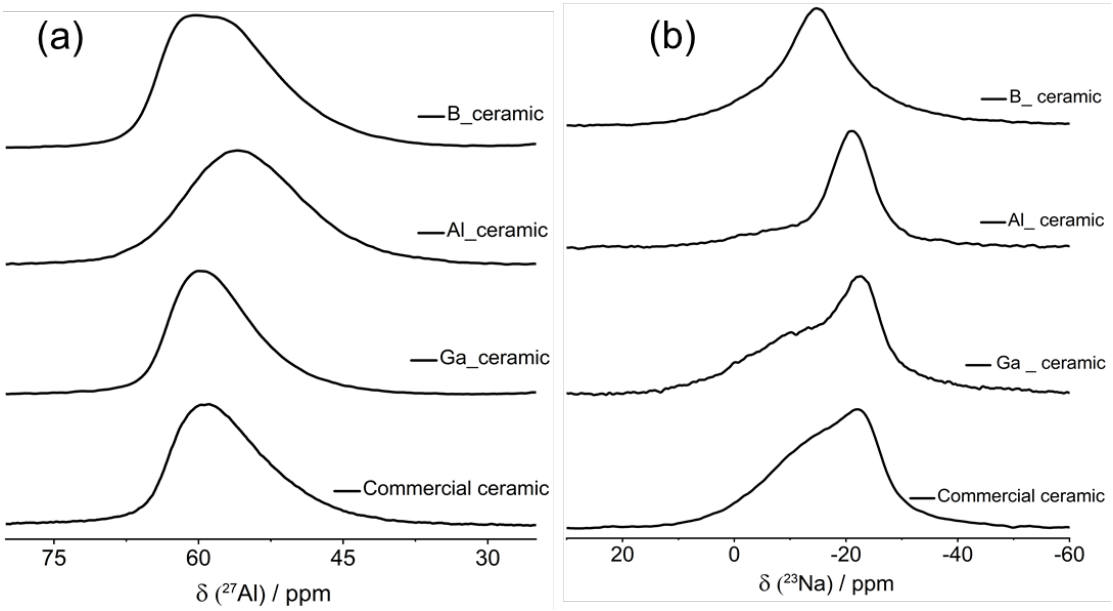


**Figure 7.** (a) $^{27}$Al ($B_0$ = 14.1 T; $\omega_r/2\pi$ = 16 kHz) and (b) $^{23}$Na ($B_0$ = 14.1 T; $\omega_r/2\pi$ = 16 kHz) MAS NMR spectra for dental ceramic VITA VM9 and synthetic samples of $Na_{0.5}K_{0.5}AlSi_3O_8$, $Na_{0.5}K_{0.5}Al_{0.9}Ga_{0.1}Si_3O_8$, and $Na_{0.5}K_{0.5}Al_{0.9}B_{0.1}Si_3O_8$.

The powder XRD patterns for these samples are similar to those of the commercial material (Figure S7). The heat treatment was adjusted slightly to mitigate the volatility of starting materials (i.e., $Na_2CO_3$ and $K_2CO_3$), followed by longer annealing to improve crystallinity. Compared to the commercial material, the broad background is less prominent in $Na_{0.5}K_{0.5}AlSi_3O_8$ and $Na_{0.5}K_{0.5}Al_{0.9}Ga_{0.1}Si_3O_8$, implying higher crystallinity, but it is still present in $Na_{0.5}K_{0.5}Al_{0.9}B_{0.1}Si_3O_8$, which is consistent with the excellent glass-forming behaviour generally found in borates. The patterns were fit to a triclinic lattice with parameters similar to those of the commercial sample (Table S1).

The $^{27}$Al MAS NMR spectra are shown in Figure 7a. Compared to the commercial material, the $^{27}$Al resonance of $Na_{0.5}K_{0.5}Al_{0.9}Ga_{0.1}Si_3O_8$ narrows slightly (Figure S8), but it is broader and shifted to higher frequency in $Na_{0.5}K_{0.5}Al_{0.9}B_{0.1}Si_3O_8$. Interestingly, the synthetic sample of $Na_{0.5}K_{0.5}AlSi_3O_8$, which underwent longer annealing, does not show a narrower peak and is

Gaussian-like, suggesting a distribution in chemical shift. Regardless of the treatment, all resonances exhibit some distribution in quadrupolar coupling characteristics, as seen in the right skewed edge of the resonance. All synthetic samples reveal the presence of some six-coordinate aluminum ($^{[6]}$Al) species with a centre-of-gravity chemical shift of $\delta_{cgs}$ = 14 ppm (Figure S9), consistent with a small amount of unreacted $Al_2O_3$ starting material, which was also apparent in the powder XRD patterns.

The $^{23}$Na NMR spectra again prove to be the most informative, providing sufficient spectral resolution between the two chemically distinct environments (Figure 7b). The synthetic sample of $Na_{0.5}K_{0.5}AlSi_3O_8$, which was annealed for 60 h, exhibits more ordered environments around the Na atoms, implying greater crystallinity and less variability in the T site, similar to previous reports [16,31]. Quantitatively, the crystalline portion ($\delta_{cgs}$ = −28 ppm) constitutes ~80% of the sample. Likewise, $Na_{0.5}K_{0.5}Al_{0.9}Ga_{0.1}Si_3O_8$ reveals two resonances, and the proportion of the crystalline component is greater for this sample than it is for the commercial sample. The spectrum of $Na_{0.5}K_{0.5}Al_{0.9}B_{0.1}Si_3O_8$ is dominated by a broad unresolved resonance in the amorphous region, which appears to represent disordered Na chemical environment. We note that the lineshape suggests the presence of two non-resolvable Na chemical environments that have similar center of gravity chemical shifts but different quadrupole coupling constants as the spectrum appears to be modeled well with a narrow and broad Gaussian lineshape (Figure S10). Combining the $^{23}$Na and $^{27}$Al NMR results leads to the conclusion that a small addition of borate hinders the onset of crystallization. Structural changes have also been reported in phosphosilicate bioglasses when incorporating small amounts of B and Al [38–40].

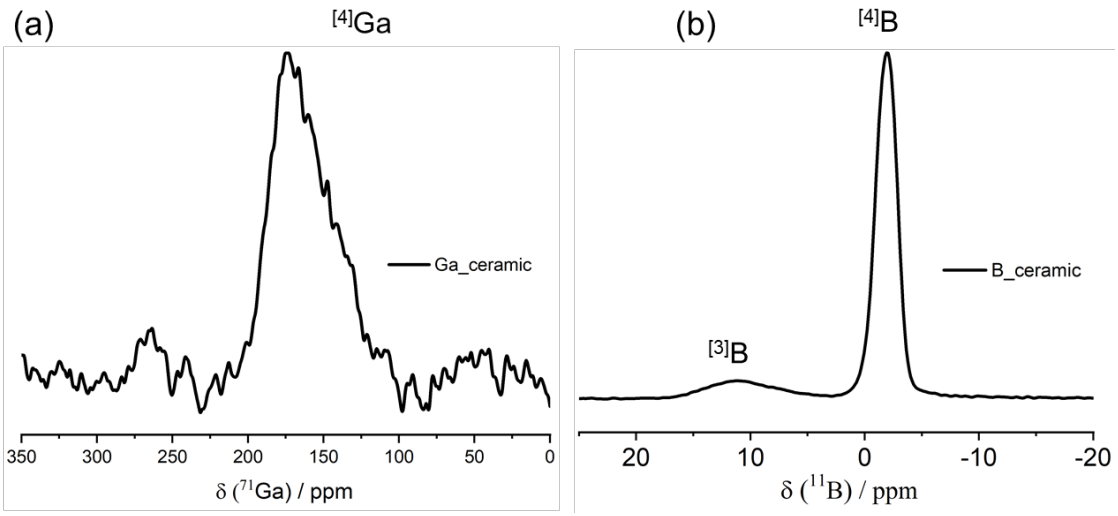


**Figure 8.** (a) $^{71}$Ga and (b) $^{11}$B MAS NMR ($B_0$ = 14.1 T; $\omega_r/2\pi$ = 16 kHz) spectra for synthetic samples for $Na_{0.5}K_{0.5}Al_{0.9}Ga_{0.1}Si_3O_8$ and $Na_{0.5}K_{0.5}Al_{0.9}B_{0.1}Si_3O_8$.

B and Ga can adopt various coordination environments in its oxides: $^{[4]}$B and $^{[3]}$B are both common in borates, whereas $^{[4]}$Ga is preferred in gallates, although $^{[6]}$Ga and $^{[5]}$Ga are occasionally found [41–43]. $^{11}$B and $^{71}$Ga MAS NMR spectra are shown for $Na_{0.5}K_{0.5}Al_{0.9}B_{0.1}Si_3O_8$ and $Na_{0.5}K_{0.5}Al_{0.9}Ga_{0.1}Si_3O_8$ (Figure 8). The $^{71}$Ga MAS NMR spectrum shows a characteristic $^{[4]}$Ga resonance with $\delta_{cgs}$ = 165±5 ppm and $C_Q$ = ~6.5±0.5 MHz (Figure 8a), consistent with other gallium-containing oxides [44-48]. The incorporation of Ga into the feldspar material results in a sizable $^{71}$Ga $C_Q$ compared to those for other Group 13 synthetic sister materials. The electric field gradient is nearly an order of magnitude larger about the $^{[4]}$Ga vs. $^{[4]}$Al when we account for the differences in both the quadrupolar frequency and the nuclear quadrupolar moment of $^{71}$Ga ($Q$ = 10.7 fm$^2$, $I$ = 3/2) and $^{27}$Al (Q = 14.66 fm$^2$, $I$ = 5/2). This finding suggests that replacing $Al^{3+}$ for the larger $Ga^{3+}$ cation within the aluminosilicate network introduces considerable $GaO_{4/2}$ polyhedral distortions, and the smaller $B^{3+}$ cation adopts a more symmetric pseudo-tetrahedral $^{[4]}$B environment as discussed below.

The $^{11}$B MAS NMR spectrum shows that $Na_{0.5}K_{0.5}Al_{0.9}B_{0.1}Si_3O_8$ contains 90 ± 2% of $^{[4]}$B and 10 ± 2% of $^{[3]}$B (Figure 8b). The chemical shifts are –2.0 ± 0.2 ppm ($C_Q$ = 0.35±0.03 MHz) for $^{[4]}$B and 14 ± 1 ppm ($C_Q$ = 2.5 ± 0.2 MHz), consistent with other borosilicates [23,48–50]. Because borates are excellent glass formers, substitution with B is less likely to induce crystallization in feldspar glass-ceramic materials under similar annealing conditions. This may provide an alternative means to control the proportions of amorphous and crystalline components in glass-ceramics while maintaining the esthetic features required for dental applications.

## Conclusions

A strategy has been demonstrated to elucidate the evolution of amorphous and crystalline components of dental glass-ceramic materials. The long-range structure of the crystalline component was probed by powder XRD, and the local structure of both the crystalline and amorphous components was probed by multinuclear solid-state magnetic resonance spectroscopy. In particular, the most useful insight into the structural changes induced by various heat treatments was provided by the $^{23}$Na NMR spectra. Quantifying the relative proportions of crystalline and amorphous components was made possible by the improved resolution in ultrahigh-field $^{23}$Na NMR spectroscopy. Alternatively, 2D MQMAS is a suitable approach at lower magnetic fields. The commercial dental material VITA VM9 contains a largely amorphous component before heat treatment, with only a minor (<30%) crystalline component. Small additions of B or Ga can change the relative amounts of these components and provides a means to control the properties of dental materials. Crystallinity is maximized between temperatures of 800 and 950 °C. These factors should thus be considered carefully in manufacturing processes.

**Acknowledgments**

This work was supported by the Natural Sciences and Engineering Research Council of Canada (NSERC, through Discovery Grants RGPIN-2016-05447 and RGPIN-2018-04294, and the Collaborative Research and Training Experience Program), Canada Foundation for Innovation, and the University of Alberta. Access to the 21.1 T NMR spectrometer was provided by the National Ultrahigh-Field NMR Facility for Solids (Ottawa, Canada), a national research facility funded by a consortium of Canadian universities and by an NSERC RTI grant, supported by NSERC and Bruker BioSpin, and managed by the University of Ottawa. We thank Dr. Victor Terskikh for assistance and scientific discussions.

## References


[1] J.R. Kelly, Dental ceramics: what is this stuff anyway? J. Am. Dent. Assoc. 139 (2008) S4–S7.

[2] J.M. Powers, R.L. Sakaguchi, R.G. Craig, Craig's restorative dental materials, 13th ed., Elsevier/Mosby, St. Louis, MO, 2012.

[3] I. Denry, J. Holloway, Ceramics for dental applications: A review, Materials 3 (2010) 351–368.

[4] Q. Chen, G. Thouas, Biomaterials: A basic introduction, 1st ed., CRC press, Taylor & Francis Group, Boca Raton, 2014.

[5] W.H. Taylor, The structure of sanidine and other feldspars, Z. Kristallogr. Cryst. Mater. 85 (1933) 425–442.

[6] H. Nekvasil, Ternary feldspar/melt equilibria: A review, I. Parsons (Ed.), Feldspars and their reactions., Springer, Netherlands, Dordrecht, 1994: pp. 195–219.

[7] M.V. Swain, Unstable cracking (chipping) of veneering porcelain on all-ceramic dental crowns and fixed partial dentures, Acta Biomater. 5 (2009) 1668–1677.

[8] A.J. Raigrodski, G.J. Chiche, N. Potiket, J.L. Hochstedler, S.E. Mohamed, S. Billiot, D.E. Mercante, The efficacy of posterior three-unit zirconium-oxide–based ceramic fixed partial dental prostheses: a prospective clinical pilot study, J. Prosthet. Dent. 96 (2006) 237–244.

[9] A.C. Diniz, R.M. Nascimento, J.C.M. Souza, B.B. Henriques, A.F.P. Carreiro, Fracture and shear bond strength analyses of different dental veneering ceramics to zirconia, Mater. Sci. Eng. C. 38 (2014) 79–84.

[10] R. Liu, T. Sun, Y. Zhang, Y. Zhang, D. Jiang, L. Shao, The effect of graded glass–zirconia structure on the bond between core and veneer in layered zirconia restorations, J. Mech. Behav. Biomed. Mater. 46 (2015) 197–204.

[11] J. Fischer, B. Stawarzcyk, A. Trottmann, C.H. Hämmerle, Impact of thermal misfit on shear strength of veneering ceramic/zirconia composites, Dent. Mater. 25 (2009) 419–423.

[12] P. Benetti, A. Della Bona, J.R. Kelly, Evaluation of thermal compatibility between core and veneer dental ceramics using shear bond strength test and contact angle measurement, Dent. Mater. 26 (2010) 743–750.

[13] S.E. Ashbrook, D.M. Dawson, NMR spectroscopy of minerals and allied materials, Nucl. Magn. Res. 45 (2016) 1–52.

[14] K.J.D. MacKenzie, M.E. Smith, Multinuclear solid-state NMR of inorganic materials, 1st ed., Pergamon, Oxford; New York, 2002.

[15] B.L. Phillips, R.J. Kirkpatrick, G.L. Hovis, $^{27}$Al, $^{29}$Si, and $^{23}$Na MAS NMR study of an Al, Si ordered alkali feldspar solid solution series, Phys. Chem. Miner. 16 (1988) 262–275.

[16] W.-H. Yang, R.J. Kirkpatrick, D.M. Henderson, High-resolution $^{29}$Si, $^{27}$Al, and $^{23}$Na NMR spectroscopic study of Al-Si disordering in annealed albite and oligoclase, Am. Mineral. 71 (1986) 712–726.

[17] J.V. Smith, C.S. Blackwell, G.L. Hovis, NMR of albite–microcline series, Nature. 309 (1984) 140.
[18] G. Engelhardt, D. Michel, High-resolution solid-state NMR of silicates and zeolites, (1987).
[19] V.K. Michaelis, P.M. Aguiar, S. Kroeker, Probing alkali coordination environments in alkali borate glasses by multinuclear magnetic resonance, J. Non-Cryst. Solids. 353 (2007) 2582–2590.
[20] R. Youngman, NMR spectroscopy in glass science: a review of the elements, Materials. 11 (2018) 476.
[21] S. Kroeker, Nuclear waste glasses: Insights from solid-state NMR, eMagRes., John Wiley & Sons, Ltd, Chichester (2007).
[22] B. Zhou, A. Faucher, R. Laskowski, V.V. Terskikh, S. Kroeker, W. Sun, J. Lin, J.-X. Mi, V.K. Michaelis, Y. Pan, Ultrahigh-field $^{25}$Mg NMR and DFT study of magnesium borate minerals, ACS Earth Space Chem. 1 (2017) 299–309.
[23] S. Kroeker, J.F. Stebbins, Three-coordinated boron-11 chemical shifts in borates, Inorg. Chem. 40 (2001) 6239–6246.
[24] Z. Xu, J.F. Stebbins, $^{6}$Li nuclear magnetic resonance chemical shifts, coordination number and relaxation in crystalline and glassy silicates, Solid State Nucl. Magn. Reson. 5 (1995) 103–112.
[25] B.R. Cherry, M. Nyman, T.M. Alam, Investigation of cation environment and framework changes in silicotitanate exchange materials using solid-State $^{23}$Na, $^{29}$Si, and $^{133}$Cs MAS NMR, J Solid State Chem. 177 (2004) 2079.
[26] V.K. Michaelis, K. Levin, Y. Germanov, G. Lelong, S. Kroeker, Ultrahigh-resolution $^{7}$Li magic-angle spinning nuclear magnetic resonance spectroscopy by isotopic dilution, Chem. Mater. 30 (2018) 5521–5526.
[27] S.E. Ashbrook, M.J. Duer, Structural information from quadrupolar nuclei in solid state NMR, Concepts Magn. Reson. Part A. 28A (2006) 183–248.
[28] R.E. Wasylishen, S.E. Ashbrook, S. Wimperis, NMR of quadrupolar nuclei in solid materials, John Wiley & Sons, 2012.
[29] J. Rodriguez-Carvajal, Recent developments of the program FULLPROF, Commission on Powder Diffraction (CPD) Newsletter 26 (2001), 12–19.
[30] C.A. Fyfe, Y. Feng, H. Grondey, G.T. Kokotailo, H. Gies, One- and two-dimensional high-resolution solid-state NMR studies of zeolite lattice structures, Chem. Rev. 91 (1991) 1525–1543.
[31] L. Zhou, J. Guo, N. Yang, L. Li, Solid-state nuclear magnetic resonance and infrared spectroscopy of alkali feldspars, Sci. China Ser. Earth Sci. 40 (1997) 159–165.
[32] J.V. Smith, C.S. Blackwell, Nuclear magnetic resonance of silica polymorphs, Nature 303 (1983) 223–225.
[33] W. Loewenstein, The distribution of aluminum in the tetrahedra of silicates and aluminates, Am. Mineral. J. Earth Planet. Mater. 39 (1954) 92–96.

[34] R. Oestrike, W. Yang, R.J. Kirkpatrick, R.L. Hervig, A. Navrotsky, B. Montez, High-resolution $^{23}Na$, $^{27}Al$ and $^{29}Si$ NMR spectroscopy of framework aluminosilicate glasses, Geochim. Cosmochim. Acta. 51 (1987) 2199–2209.

[35] E. Lippmaa, A. Samoson, M. Magi, High-resolution aluminum-27 NMR of aluminosilicates, J. Am. Chem. Soc. 108 (1986) 1730–1735.

[36] D.R. Neuville, L. Cormier, D. Massiot, Al environment in tectosilicate and peraluminous glasses: a $^{27}Al$ MQ-MAS NMR, Raman, and XANES investigation, Geochim. Cosmochim. Acta. 68 (2004) 5071–5079.

[37] R.K. Harris, E.D. Becker, S.M.C. De Menezes, R. Goodfellow, P. Granger, NMR nomenclature. Nuclear spin properties and conventions for chemical shifts (IUPAC Recommendations 2001), Pure Appl. Chem. 73 (2001) 1795–1818.

[38] L. Deilmann, O. Winter, B. Cerrutti, H. Bradtmüller, C. Herzig, A. Limbeck, O. Lahayne, C. Hellmich, H. Eckert, D. Eder, Effect of boron incorporation on the bioactivity, structure, and mechanical properties of ordered mesoporous bioactive glasses, J. Mater. Chem. B 8 (2020) 1456–1465.

[39] S. Melchers, T. Uesbeck, O. Winter, H. Eckert, D. Eder, Effect of Aluminum ion incorporation on the bioactivity and structure in mesoporous bioactive glasses, Chem. Mater. 28 (2016) 3254–3264.

[40] Y. Yu, B. Stevensson, M. Edén, Medium-range structural organization of phosphorus-bearing borosilicate glasses revealed by advanced solid-state NMR experiments and MD simulations: consequences of B/Si substitutions, J. Phys. Chem. B 121 (2017) 9737–9752.

[41] P.J. Bray, NMR and NQR studies of boron in vitreous and crystalline borates, Inorg. Chim. Acta. 289 (1999) 158–173.

[42] P.J. Bray, G.L. Petersen, NMR and NQR studies of borate glasses, Z. Naturforsch. A 53 (1998) 273–284.

[43] P.E. Stallworth, P.J. Bray, Nuclear magnetic resonance in glass, Glass science and technology, vol. 4B, Academic Press, Orlando (1990), pp. 77-149.

[44] D. Massiot, I. Farnan, N. Gautier, D. Trumeau, A. Trokiner, J.P. Coutures, $^{71}Ga$ and $^{69}Ga$ nuclear magnetic resonance study of β-$Ga_2O_3$: resolution of four-and six-fold coordinated Ga sites in static conditions, Solid state Nucl. Magn. Reson. 4 (1995) 241–248.

[45] P. Hee, R. Christensen, Y. Ledemi, J.E. Wren, M. Dussauze, T. Cardinal, E. Fargin, S. Kroeker, Y. Messaddeq, Properties and structural investigation of gallophosphate glasses by $^{71}Ga$ and $^{31}P$ nuclear magnetic resonance and vibrational spectroscopies, J. Mater. Chem. C 2 (2014) 7906–7917.

[46] T. Skopak, S. Kroeker, K. Levin, M. Dussauze, R. Méreau, Y. Ledemi, T. Cardinal, E. Fargin, Y. Messaddeq, Structure and properties of gallium-rich sodium germano-gallate glasses, J. Phys. Chem. C. 123 (2019) 1370–1378.

[47] T. Skopak, P. Hee, Y. Ledemi, M. Dussauze, S. Kroeker, T. Cardinal, E. Fargin, Y. Messaddeq, Mixture experimental design applied to gallium-rich $GaO_{3/2}$-$GeO_2$-$NaO_{1/2}$ glasses, J. Non-Cryst. Solids. 455 (2017) 83–89.

[48] S. Sen, Z. Xu, J.F. Stebbins, Temperature dependent structural changes in borate, borosilicate and boroaluminate liquids: high-resolution $^{11}B$, $^{29}Si$ and $^{27}Al$ NMR studies, J. Non-Cryst. Solids. 226 (1998) 29–40.

[49] L.-S. Du, J.F. Stebbins, Nature of silicon−boron mixing in sodium borosilicate glasses: A high-resolution $^{11}B$ and $^{17}O$ NMR study, J. Phys. Chem. B 107 (2003) 10063–10076.

[50] W.J. Dell, P.J. Bray, S.Z. Xiao, $^{11}B$ NMR studies and structural modeling of $Na_2O$-$B_2O_3$-$SiO_2$ glasses of high soda content, J. Non-Cryst. Solids. 58 (1983) 1–16.